is an example. The PVFer is spatially isolated from the Pt surface by the poly[Ru(vbpy)$_3$]$^{2+}$ film, forcing its oxidation reaction to occur near the electrode potential for Ru(III) production, by the mediation reaction

$$\text{poly[Ru(vbpy)}_3\text{]}^{3+} + \text{PVFer} \rightarrow \text{poly[Ru(vbpy)}_3\text{]}^{2+} + \text{PVFer}^+ \quad (7)$$

which is called a (ferrocenium) charge-*trapping* reaction.

The trapped PVFer$^+$ state is stable for considerable periods when the poly[Ru(vbpy)$_3$]$^{2+}$ inner film layer is reasonably thick. We were interested in how *thin* the inner film thickness could be, yet still effect the charge-trapping reaction 7 at all (as opposed to direct oxidation of PVFer by the Pt electrode), and how rapidly PVFer$^+$ trapped states formed when using very thin inner films leak away. Figure 10 shows a cyclic voltammogram where Γ_T for the inner film poly[Ru(vbpy)$_3$]$^{2+}$ layer was only 6×10^{-10} mol/cm^2, or ca. 40 Å. The initial positive potential scan shows only a small anodic current inflection at ca. +0.44 V vs. SSCE (the thermodynamic potential for PVFer oxidation in acetonitrile) and then a large current peak at +0.93 V (curve E) from previous studies we know to be the trapping reaction.[1,2] This result demonstrating charge trapping for very thin inner layers is significant in that switching times for these film assemblies as charge rectifying or as stably switched electrochromic surfaces[5] are thereby predicted for equally thin outer films to be as short as (by the approximate thickness relation, $(D_{ct}t)^{1/2}$) ca. 1 ms.

Following scanning through the poly[Ru(vbpy)$_3$]$^{3+/2+}$ wave at +1.1 V, no reverse wave for PVFer$^+$ reduction is seen (as expected[1,2]). If the potential is scanned again positively from 0 V immediately or after pause-waiting periods of 1, 2, or 4 min (curves A–D), a retrapping peak is observed near +0.9 V whose magnitude does not increase proportionately to the waiting time. This indicates that leakage does occur for this thin inner film but not all regions of the film leak away charge at equal rates.

The wave at ca. +0.44 V in Figure 10 is notable both for its small size and its shape. The charge under the +0.44-V wave is <5% of the +0.93-V initial charge-trapping peak; very little ferrocene is oxidized by permeation through the inner poly[Ru(vbpy)$_3$]$^{2+}$ film. That which is oxidized gives a membrane diffusion cyclic voltammetric shape reminiscent of that in Figure 9, curve D, which implies that slow diffusion of PVFer chains into the poly[Ru(vbpy)$_3$]$^{2+}$ polymer can occur on a time scale of 1 s or so. However, this polymer/polymer interpenetration does not over the course of time homogenize the films (else no trapping peak at all), so the PVFer diffusion must more resemble a large-scale polymer segmental vibration than a net diffusional mass transport. This particular observation is of interest with respect to the stability of bilayer polymer film assemblies and the kinetics of electron-transfer trapping reactions at the polymer/polymer poly[Ru(vbpy)$_3$]$^{3+}$/PVFer interface.[70]

Conclusions

This paper demonstrates the feasibility of electrochemically preparing ultrathin redox polymer films which exhibit both molecular size and charge discrimination toward solutes in contact with them. This observation is significant in that the ruthenium polymers have redox properties making them potential oxidation catalysts for electroorganic reactions; their permeability characteristics also suggest the possibility of size *selective* oxidation processes by the polymer, and/or by the underlying electrode or other catalyst. The discrimination of molecular size is, crudely, comparable to that of zeolitic structures.[10,11]

Acknowledgment. This research was supported in part by grants from the National Science Foundation and the Office of Naval Research.

Registry No. [Ru(vbpy)$_3$]$^{2+}$, 75675-24-0; [Ru(bpy)$_2$(p-cinn)$_2$]$^{2+}$, 81205-89-2; VDQ^{2+}, 78099-25-9; poly[Ru(vbpy)$_3$]$^{2+}$, 81206-05-5; poly[Ru(bpy)$_2$(p-cinn)$_2$]$^{2+}$, 81206-06-6; poly[VDQ]$^{2+}$, 78099-26-0; [Ru(bpy)$_2$Cl$_2$], 15746-57-3; [Fe(bpy)$_2$(CN)$_2$], 14841-10-2; [Ru(bpy)$_2$(py)Cl]$^+$, 33519-09-4; [Ru(bpy)$_3$]$^{2+}$, 15158-62-0; bromide, 24959-67-9; *p*-benzoquinone, 106-51-4; ferrocene, 102-54-5; diquat^{2+}, 2764-72-9.

(70) Denisevich, P.; Willman, K.; Murray, R. W., unpublished results.

Electronic Structure of Naphtho[1,8-*cd*:4,5-*c'd'*]bis[1,2,6]thia- and -selenadiazines. Ab Initio Calculations and Photoelectron Spectra

J. P. Boutique,*[†,§] J. Riga,[†] J. J. Verbist,[†] J. Delhalle,[†] J. G. Fripiat,[‡] J. M. Andre,[‡] R. C. Haddon,[∥] and M. L. Kaplan[∥]

Contribution from the Universitaires Notre-Dame de la Paix, B-5000 Namur, Belgium, and Bell Laboratories, Murray Hill, New Jersey 07974. Received September 16, 1981

Abstract: The electronic structure and related ground-state properties of naphtho[1,8-*cd*:4,5-*c'd'*]bis[1,2,6]thiadiazine and naphtho[1,8-*cd*:4,5-*c'd'*]bis[1,2,6]selenadiazine have been investigated by means of both theoretical and experimental approaches. X-ray photoelectron spectra of the C 1s, N 1s, S 2p (and Se 3p) core levels provide information on the atomic-charge distribution in the C–N–S(Se)–N–C region. Ab initio STO-3G calculations reveal a drastic perturbation of the electron-density distribution in the naphthalene skeleton. This theoretical model fits the experimental results very well and clearly explains the XPS valence band data.

Introduction

The discovery in 1975 of the first superconducting polymeric material,[1] $(SN)_x$, has induced a search for related compounds having one or several NXN groups (X = S, Se) attached in a similar way as in $(SN)_x$. Several systems such as X–nitrogen heterocycles and classical aromatics bridged by NXN group(s) have displayed rather unusual physicochemical properties and thereby drawn attention to the NXN linkage.

Naphtho[1,8-*cd*:4,5-*c'd'*,]bis[1,2,6]thiadiazine and naphtho[1,8-*cd*:4,5-*c'd'*]bis[1,2,6]selenadiazine, schematically represented

[†] Laboratoire de Spectroscopie Electronique, Universitaires Notre-Dame de la Paix.
[‡] Laboratoire de Chimie Theorique Appliquee Facultes, Universitaires Notre-Dame de la Paix.
[§] Holder of a followship of IRSIA, Belgium.
[∥] Bell Laboratories.

(1) Green, R. L.; Grant, P. M.; Street, G. B. *Phys. Rev. Lett.* **1975**, *34*, 89.

0002-7863/82/1504-2691$01.25/0

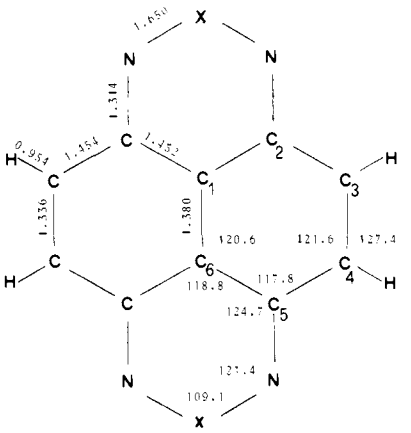

Figure 1. Schematic molecular structure of $(NXN)_2$ (X = S, Se). Bond lengths (Å) and angles (deg) are given for $(NSN)_2$ from ref 3.

in Figure 1 and referred to as $(NSN)_2$ and $(NSeN)_2$, respectively, in the following, are most interesting in this context because of their somewhat contradictory properties.[2,3] For instance, $(NSN)_2$ exhibits a strong chemical stability indicative of aromatic character while its ^1H NMR chemical shift, electrochemistry, electronic spectrum, and crystal structure suggest the opposite. Similarly, Yavari et al.[4] argue in favor of the participation of sulfur 3d orbitals to explain the high-field position of the ^{15}N resonance of the related naphtho[1,8-*cd*][1,2,6]thiadiazine, while others tend to disagree on the basis of similarities between UPS spectra of thiadiazines and triazines.[5] The present knowledge of the groundstate electronic structure of $(NSN)_2$ and $(NSeN)_2$ can be further improved with the help of X-ray photoelectron spectroscopy (XPS) and quantum mechanical calculations; indeed a combination of XPS and theory offers one of the most powerful methods of studying charge distributions and electronic energy level characteristics.

In this paper, we present an analysis of $(NSN)_2$ and $(NSeN)_2$ XPS spectra on the basis of STO-3G and STO-3G+5D ab initio calculations on $(NSN)_2$, a theoretical investigation on $(NSeN)_2$ being presently out of our reach.

Experimental Section

XPS Measurements. The compounds $(NSN)_2$ and $(NSeN)_2$ were prepared according to literature methods.[2,6] After being crushed, samples were pressed in pellet form on a gold substrate.

XPS spectra were recorded at ambient temperature with a Hewlett-Packard 5950A spectrometer, with monochromatized Al $K\alpha_{1,2}$ radiation ($h\nu$ = 1486.6 eV) as incident source. During data acquisition, the pressure in the sample chamber was about 2×10^{-9} torr. Due to emission of photoelectrons we used the flood-gun technique to neutralize positive charge buildup effects at the sample surface. During the measurement the oxygen contamination remained very small as checked on the O 1s signal evolution. Because of concern with possible degradation of the sample surface due to the gold decoration technique, absolute calibration of the spectra was performed by admixing polyethylene to the sample. The C 1s polyethylene binding energy was found at 284.6 eV by reference to the Au $4f_{7/2}$ level (84.0 eV). Except in Figure 8, all spectra presented in this paper were smoothed by a least-squares procedure based on a second-degree polynomial involving nine points at a time.

Theoretical Calculations

Restricted Hartree–Fock Roothaan (LCAO-SCF-MO) results on $(NSN)_2$, at a geometry slightly modified from its known crystal structure[3] so as to accommodate D_{2h} symmetry (see Figure 1 for details), have been obtained with STO-3G and STO-3G + 5D basis sets by using the GAUSSIAN 76 program.[7] All integrals larger than 10^{-6} were explicitly taken into account, and the convergence threshold on density matrices was less than 5.10^{-4}. The STO-3G and STO-3G+5D bases (five d orbitals contracted from six Cartesian functions) are identical with the ones developed by Pople and co-workers for third-row atoms.[8] Due to the controversy regarding their necessity in computations, we considered d orbitals in this work to study their influence on the NSN bonding description as well as on the one-electron levels. In spite of the known limitations of STO-3G and STO-3G+5D bases, a choice that was merely dictated by computing constraints, we decided to rely on them to compute charge distribution indices and correlate XPS spectra with orbital energies. This attempt is supported by the results on a series of sulfur nitrides obtained by Findlay et al.[9] where they correlated XPS data with better than double-ζ calculations and analyzed results from minimal basis sets (sp, spd) and semiempirical methods.

Our correlations of the spectral and calculated data are based on Koopmans' theorem, and to enlarge our basis of interpretation we simulated the experimental spectrum from theoretical results. According to Gelius's model[10] the intensity of the jth one-electron state, I_j, is a weighted sum of products of atomic gross populations, $P_{A\lambda_j}$, with the corresponding atomic orbitals (AO) relative cross-sections $\sigma^{AO}_{A\lambda}/\sigma^{AO}_{A_0\lambda_0}$:

$$I_j \propto + (2 + \beta/2) \sum_{A,\lambda} P_{A\lambda j} \frac{\sigma^{AO}_{A\lambda}}{\sigma^{AO}_{A_0\lambda_0}}$$

where λ is the angular momentum of the atomic orbital A and β is an asymmetry parameter for the molecular orbital j. For each molecular orbital, the sum was extended over all the valence atomic orbitals. Only the STO-3G basis was used, and the symmetry parameter β was arbitrarily fixed to 2 for each molecular orbital. The theoretical spectrum is made out of a series of peaks located at each one electron eigenvalue, ϵ_j, on the energy scale. Their shape is a combination of one Lorentzian and one Gaussian having both the same intensity and width (1.5 eV) over the entire spectrum. The resulting valence band has been linearly contracted on the energy scale to obtain the best overall fit with experiment. A sigmoid background, locally dependent on the peak intensity, has been subtracted from the original spectrum.

Calculations reported in this work were carried out on the DEC 2060 computer of the Facultès Universitaires Computing Center.

Theoretical Results

In this part, we first investigate electron density distribution changes in the naphthalene skeleton due to the bridging by NSN groups and then analyze the bonding character of the one-electron levels that will be correlated with experimental data in the next section.

The electron density distribution is conveniently described in the framework of the Mulliken population analysis. Though artificial, we also considered in this discussion an intermediary structure made out of the unperturbed naphthalene skeleton bridged by two NSN groups having the same geometry as in $(NSN)_2$. The values for the intermediary structure are given in parentheses. Table I collects molecular total energies and gross atomic and overlap populations. Since no geometry optimization was carried out, total energies are reported here for indicative purpose only; extension of the STO-3G basis to include d orbitals on sulfur atoms yields lower values, and the intermediary structure is found less stable than the experimental one by 12.5 kcal mol^{-1} at the STO-3G level. The STO-3G calculations predict important

(2) Haddon, R. C.; Kaplan, M. L.; Marshall, J. H. *J. Am. Chem. Soc.* **1978**, *100*, 1235.
(3) Gieren, A.; Lamm, V.; Haddon, R. C.; Kaplan, M. L. *J. Am. Chem. Soc.* **1979**, *101*, 7277.
(4) Yavari, I.; Botto, R. E.; Roberts, J. D. *J. Org. Chem.* **1978**, *43*, 2542.
(5) Bartetzko, R.; Gleiter, R. *Angew. Chem., Int. Ed. Engl.* **1978**, *17*, 468.
(6) Kaplan, M. L.; Haddon, R. C.; Schilling, F. C.; Marshall, J. H.; Bramwell, F. B. *J. Am. Chem. Soc.* **1979**, *101*, 3306.
(7) Pople, J. A.; Binkley, J. S.; Whitehead, R. A.; Hariharan, P. C.; Seeger, R. *QCPE* **1978**, *10*, 368.
(8) (a) Hehre, W. J.; Ditchfield, R.; Stewart, R. F.; Pople, J. A. *J. Chem. Phys.* **1970**, *52*, 2769. (b) Collins, J. B.; Schleyer, P. v. R.; Binkley, J. S.; Pople, J. A. *Ibid.* **1976**, *64*, 5142.
(9) Findlay, R. H.; Palmer, H. H.; Downs, A. J.; Egdell, R. G.; Evans, R. *Inorg. Chem.* **1980**, *19*, 1307.
(10) (a) Gelius, U. "Electron Spectroscopy"; Shirley, D. A., Ed.; North-Holland, Amsterdam, 1972, 311. (b) Gelius, U. *J. Electron Spectrosc. Relat. Phenom.* **1974**, *5*, 985.

Table I. Theoretical Calculations on $(NSN)_2$: Total Energies, Electronic Charges, and Mulliken Overlap Populations[a]

	STO-3G	STO-3G+5D	naphthalene STO-3G results
total energies, au	−1377.496 079 (−1377.475 992)	−1377.659 941	
electronic charges[b]			
S	15.54 (15.55)	15.73	
N	7.34 (7.33)	7.25	
C_1	6.03 (6.02)	6.02	6.00
C_2	5.91 (5.93)	5.89	6.06
C_3	6.08 (6.04)	6.08	6.06
Mulliken overlap populations[c,d]			
$3p_z$–$2p_z$: S–N	0.018 (0.019)	0.021	
$2p_z$–$2p_z$: N–C_2	0.151 (0.142)	0.145	
C_1–C_2	0.034 (0.039)	0.035	0.072
C_2–C_3	0.030 (0.051)	0.032	0.143
C_3–C_4	0.176 (0.139)	0.175	0.071
C_1–C_6	0.145 (0.136)	0.143	0.017
$S3d_{xz}$–$N2p_z$		0.015	
$S3d_{yz}$–$N2p_z$		0.008	

[a] Values in parentheses refer to calculations on the intermediary structure. [b] Carbon atoms are labeled as in Figure 1. [c] The π C $2p_z$–C $2p_z$ overlap population between adjacent carbons in benzene is 0.110. [d] From ref 3, the π-bond orders are as follows: S–N, 0.18; N–C_2, 0.77; C_1–C_2, 0.33; C_2–C_3, 0.32; C_3–C_4, 0.95; C_1–C_6, 0.71.

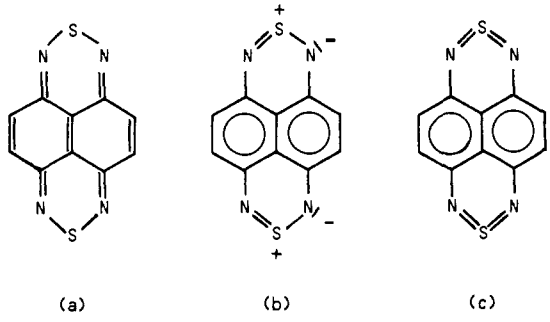

Figure 2. Resonance formulas proposed for $(NSN)_2$.

electron migration from sulfur to nitrogen, but only those carbons linked to nitrogen atoms are influenced and they become positively charged. From gross atomic populations, it seems as if the NSN linkage induces no change on the naphthalene skeleton; C_1 and C_3 keep their free-atom gross atomic populations. In agreement with previous study on $(SN)_x$ oligomers,[11] inclusion of d orbitals decreases substantially the NSN bond polarity but holds the C_1, C_2, and C_3 charges at their STO-3G values.

On the contrary, overlap populations reflect essential modifications in the naphthalene skeleton caused by the NSN groups. It is interesting to observe that in the intermediary structure, where no geometry relaxation is allowed, most of the modifications are already present. One can notice important π overlap populations between carbon and nitrogen atoms as well as for all bonds parallel to the C_2 axis joining the two sulfur atoms. The π-bond character of the other bonds remains unchanged or is decreased; this is in agreement with the π-bond-order sequences derived from the crystal structure.[3] The main result of the bridging is a complete alteration of the double and single bonds pattern in the carbon framework as compared to naphthalene, as can also be seen by correlating the overlap population values and geometry of the three molecules: naphthalene, $(NSN)_2$, and the intermediary structure. S $3p_z$–N $2p_z$ overlap population is slightly influenced by 3d sulfur orbitals, but as seen in Table I, S $3d_{xz}$–N $2p_z$ and S $3d_{yz}$–N $2p_z$ contributions have values comparable with S $3p_z$–N $2p_z$.

The results of the population analysis support a quinonoid-type structure (Figure 2a) as more appropriate than other resonance formulas (Figure 2b,c) to describe $(NSN)_2$ bonds. Overlap populations exhibit strong alternation, indicative of low π-electron delocalization over the molecular framework compared to what is expected in a fully aromatic situation.

Table II gives orbital energies, the symmetry, and the dominant bonding character ($s\sigma$, $p\sigma$, $p\pi$, ...) of the molecular orbitals. Figure 3 provides a schematic representation of the π one-electron states

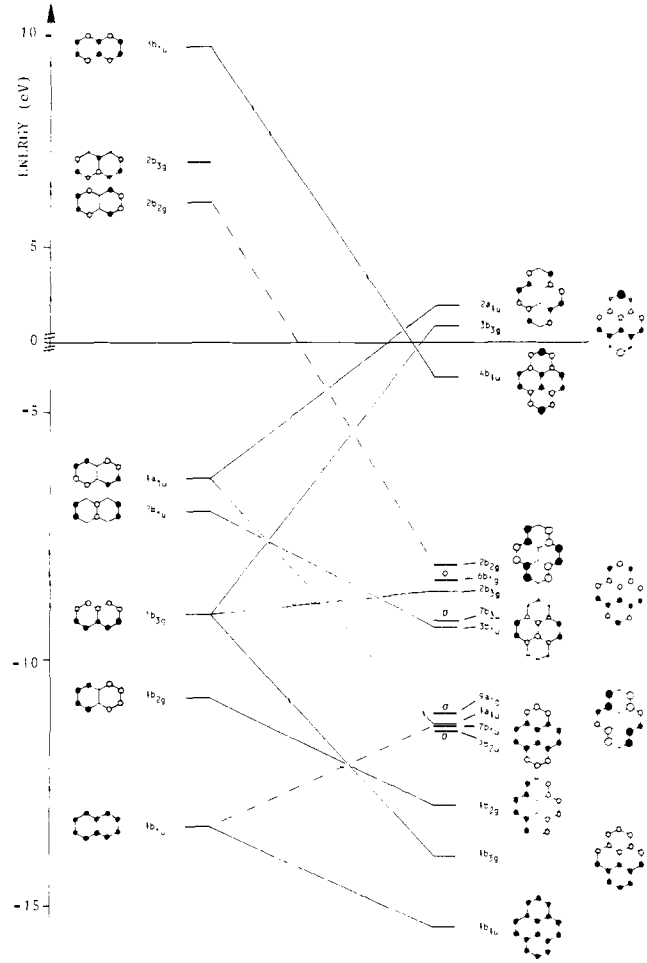

Figure 3. Evolution of the π electronic levels from naphthalene to $(NSN)_2$.

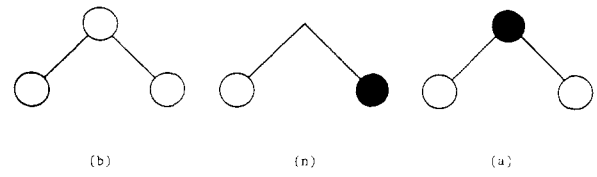

Figure 4. Combinations of the π orbitals of the NSN linkage.

Table II. Monoelectronic Energy Levels of $(NSN)_2$

level (D_{2h})	character	energy, eV STO-3G	STO-3G+5D
$1a_{1g}$	sσ	34.31	33.88
$1b_{2u}$	sσ	34.05	33.57
$1b_{3u}$	sσ	31.97	31.77
$1b_{1g}$	sσ	31.62	31.39
$2a_{1g}$	sσ	30.29	30.03
$2b_{3u}$	sσ	28.43	28.33
$3a_{1g}$	sσ	27.38	27.29
$2b_{2u}$	sσ	27.04	26.68
$4a_{1g}$	sσ	24.11	*23.78*
$2b_{1g}$	sσ	23.98	23.90
$3b_{2u}$	sσ	22.97	22.86
$3b_{3u}$	sσ	22.19	22.11
$4b_{2u}$	sσ	21.21	21.03
$3b_{1g}$	sσ	19.22	19.12
$4b_{3u}$	pσ	18.87	18.81
$5a_{1g}$	pσ	18.13	18.09
$6a_{1g}$	pσ	17.76	17.66
$4b_{1g}$	pσ	16.27	16.21
$7a_{1g}$	sσ	16.09	16.02
$5b_{3u}$	pσ	15.54	15.49
$1b_{1u}$	pπ	15.39	15.24
$6b_{3u}$	pσ	15.25	15.11
$5b_{2u}$	pσ	15.09	15.08
$1b_{3g}$	pπ	13.93	13.75
$5b_{1g}$	pσ	13.07	12.97
$1b_{2g}$	pπ	12.91	12.82
$6b_{2u}$	sσ	12.08	12.15
$8a_{1g}$	pσ	11.57	11.56
$7b_{2u}$	pσ	11.39	11.42
$2b_{1u}$	pπ	11.31	*11.03*
$1a_{1u}$	pπ	11.26	11.15
$9a_{1g}$	pσ	11.02	11.09
$3b_{1u}$	pπ	9.34	9.23
$7b_{3u}$	pσ	9.17	9.12
$2b_{3g}$	pπ	8.64	*8.19*
$6b_{1g}$	pσ	8.37	8.31
$2b_{2g}$	pπ	8.08	8.08
$4b_{1u}$	pπ	4.30	3.85

of both naphthalene and $(NSN)_2$.

The low-lying $(NSN)_2$ valence π levels may be regarded as resulting from interactive mixing of naphthalene π orbitals with the three possible symmetric combinations of p_z orbitals located on the atoms of the NSN group. These combinations are shown in Figure 4 and labeled b, n, and a, respectively, for bonding, nonbonding, and antibonding. It should be noted that d orbitals on sulfur are of the correct symmetry for mixing with the n orbital.[11] A bonding combination of a with $1b_{1u}$, $1b_{3g}$, and $2b_{1u}$ of naphthalene leads to the highly stabilized $1b_{1u}$, $1b_{3g}$, and $3b_{1u}$ levels of $(NSN)_2$. Similarly, the bonding mixture of n with $1b_{2g}$, $1a_{1u}$, and $2b_{2g}$ gives $1b_{2g}$, $1a_{1u}$, and $2b_{2g}$ in $(NSN)_2$. The $2b_{1u}$ of $(NSN)_2$ may be seen as an antibonding interaction of b with $1b_{1u}$ of naphthalene, while $2b_{3g}$ of $(NSN)_2$ comes out from a mixture of a with $1b_{3g}$ of naphthalene. Beyond that point it becomes more difficult to identify the combinations in such a straightforward way. Let us point out that the two highest occupied levels in $(NSN)_2$, $2b_{2g}$ and $4b_{1u}$, are completely different from those in naphthalene, i.e., $2b_{1u}$ and $1a_{1u}$. The strong antibonding mixture of the naphthalene $1a_{1u}$ level with n promotes the resulting molecular orbital in the unoccupied part of the $(NSN)_2$ spectrum, while the unoccupied $2b_{2g}$ and $3b_{1u}$ molecular orbitals of naphthalene are strongly stabilized by a bonding admixture of n and a, respectively.

The highest levels of σ character, $6b_{1g}$ and $7b_{3u}$, are located at 8.37 and 9.17 eV and correspond mainly to the N $2p_x \pm$ S $3p_x$ combination. The $9a_{1g}$ and $7b_{2u}$ σ molecular orbitals, found at 11.02 and 11.39 eV, have a N $2p_y \pm$ S $3p_y$ dominant character. Levels describing C–H, C–C, and C–N bonds are much lower in the energy spectrum and have not been drawn in Figure 4 for the sake of clarity.

In the occupied region of the energy spectrum, 3d sulfur orbitals enter the LCAO expansion with small coefficients, and as seen from Table II, STO-3G and STO-3G+5D levels follow the same symmetry sequence except for the three cases given in italics. This is very similar to what was found by Findlay et al. in their study on SN, S_2N_2, and S_4N_4.[9] Besides the four lowest valence-energy levels ($1a_{1g}$, $1b_{2u}$, $1b_{3u}$, $1b_{1g}$), $2b_{3g}$, and the highest occupied $4b_{1u}$ molecular level, all STO-3G orbital energies are energetically close to the STO-3G+5D ones. Though not explicitly tabulated here, the first unoccupied levels exhibit large 3d contributions which markedly influence their position on the energy scale.

Table III. Core- and Valence-Peak Binding Energies of $(NSN)_2$ (eV)

core peak	peak position	satellite position (intensity)
C 1s	284.4–285.6	289.2 (low)
N 1s	398.6	399.6 (strong)
		402.4 (low)
S $2p_{3/2}$	164.5	166.9 (low)
S $2p_{1/2}$	165.7	168.1 (low)

valence peak[a]	peak position	valence peak	peak position
A	1.4	E	11.1
B	3.8	F	15.3
C	6.2	G	17.1
D	9.0	H	22.5

[a] Peaks are labeled as in Figure 8.

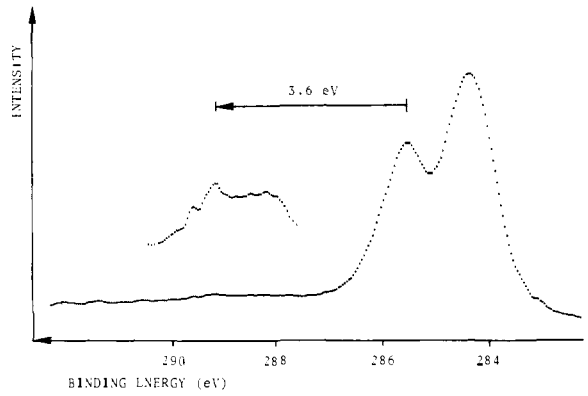

Figure 5. X-ray photoelectron spectrum of the C 1s level in $(NSN)_2$.

Experimental Results

Hereafter we analyze the spectral XPS characteristics (core levels, valence band, and satellites) of $(NSN)_2$ and $(NSeN)_2$ respectively in A and B; N 1s core peak shapes are discussed in (C).

A. $(NSN)_2$. Core Levels. Their characteristics are summarized in Table III. The C 1s peak shows two components with a 4:6 intensity ratio (Figure 5), respectively located at 285.6 and 284.4 eV. By reference to the gross atomic populations, we assign the higher binding energy component to the four positive carbons linked to nitrogen (C_α). The calculated core levels describing the C 1s orbitals are found at 302.28 (C_2, C_5, C_7, C_{10}), 301.20 (C_1, C_6), and 301.02 eV (C_3, C_4, C_8, C_9). The 1.20-eV separation between the C 1s orbital energy of carbons linked to nitrogens (302.28 eV) and the average over the other C 1s orbital energies (301.08 eV) is in excellent agreement with the experimental splitting (see Table III). A satellite is found at 289.2 eV.

The N 1s peak arises at 398.6 eV (Figure 6). The correlation established by Nordberg[12] between the position of the N 1s line and the calculated charge locates neutral nitrogen at 399.4 eV.

(11) Haddon, R. C.; Wasserman, S. R.; Wudl, F.; Williams, G. R. J. *J. Am. Chem. Soc.* **1980**, *102*, 5070.

(12) Nordberg, R.; Albridge, R. G.; Bergmark, T.; Ericson, U.; Hedman, J.; Nordling, C.; Siegbahn, K.; Lindberg, B. J. *Arkiv Kemi* **1968**, *28*, 257.

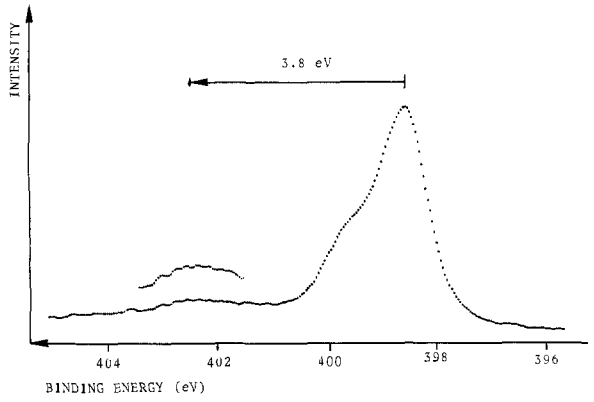

Figure 6. X-ray photoelectron spectrum of the N 1s level in $(NSN)_2$.

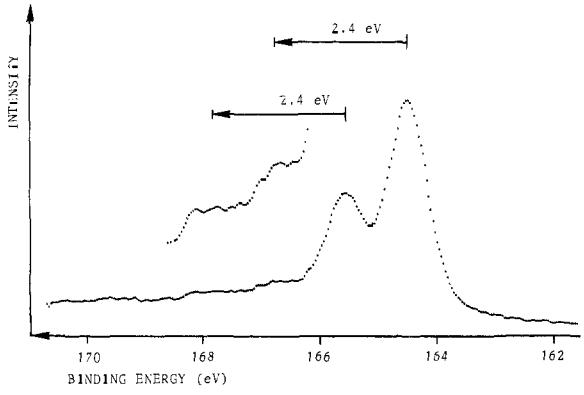

Figure 7. X-ray photoelectron spectrum of the S 2p levels in $(NSN)_2$.

The shift observed in our compound is indicative of high electron density or partial negative charge on nitrogen. A large shoulder is found on the high-energy side of the N 1s signal, and a weak satellite appears at 402.4 eV.

The S 2p doublet (Figure 7) appears simple and well resolved, indicating two equivalent sulfur atoms. In agreement with theoretical findings, its high binding energy reflects electron deficiency on sulfurs compared to that in cyclooctasulfur [E_B(S $2p_{3/2}$) = 164.2 eV].[13] With each S 2p peak is associated a low-intensity satellite 2.4 eV from the main peak.

Valence Levels. Their essential features are listed in Table III; the valence-band spectrum is given in Figure 8. The peak A, located at 1.4 eV, corresponds to the $4b_{1u}$ π level. Its high intensity is explained by a strong S 3p character. In peak B, starting from lower binding energies, one can identify the following π levels: $2b_{2g}$ (C=N double bonds), $2b_{3g}$ with important S 3p contributions, and $3b_{1u}$. These π levels overlap with the intense $6b_{1u}$ and $7b_{3u}$ levels describing the S $3p_{x,y} \pm$ N $2p_{x,y}$ combinations of atomic orbitals.

An intense peak at 6.2 eV, C in Figure 8, contains several σ molecular orbitals ($9a_{1g}$, $7b_{2u}$, $8a_{1g}$, $6b_{2u}$) with important S $3p_x$, S $3p_y$, N $2p_x$, and N $2p_y$ contributions. They describe mainly the pσ S–N bonds, the nitrogen and sulfur lone pairs lying in the molecular plane.

The weaker π $1b_{2g}$ and σ $5b_{1g}$ levels are located between the C and D peaks. The energy region extending from 8 to 13 eV contains essentially the pσ-type levels and those referring to the C $2p_{x,y}$–H 1s interactions. The sσ molecular orbitals (peaks E, F, G, H) appear at higher binding energies.

The theoretical simulation reproduces correctly the relative positions and intensities of these peaks (Figure 8). The overvaluation of the sσ orbital intensities is likely due to the use of Mulliken gross atomic populations, which enhance the s contributions instead of net populations,[10b] and to the fixed line width (1.5 eV) assumed over the entire spectrum. This is clearly seen

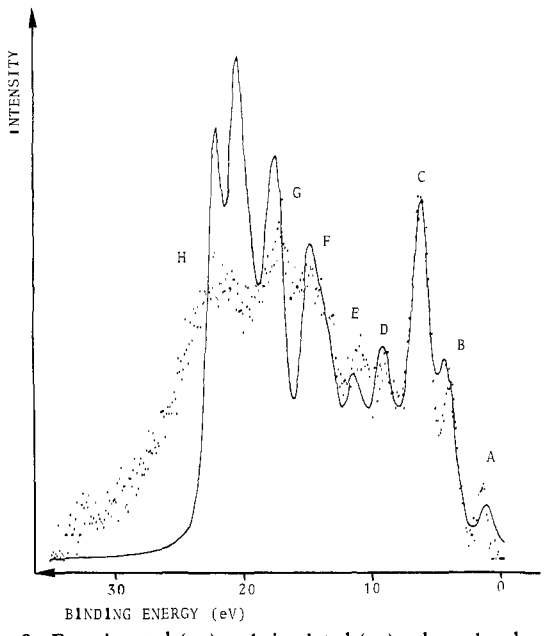

Figure 8. Experimental (···) and simulated (—) valence-band spectra of $(NSN)_2$.

for the N 2s level at around 22 eV; the theoretical simulation predicts it to be too narrow and too high compared with the experimental line.

Satellites. If we except the shoulder on the left-hand side of the N 1s signal (399.6 eV) that we will discuss in C, all the other observed structures in the core level spectrum are interpreted as resulting from a shake-up process. This ionization–excitation process is here described in the simplified one-electron picture.[14,15] Therefore we will focus only on the starting orbitals, without attempt to reach the involved excited levels: that would require sophisticated calculations taking into account many-electron effects.[16] Following the core ionization, the molecular orbitals relax suddenly to screen the photo hole. This relaxation energy may induce a simultaneous excitation of a valence electron to an empty level of the same symmetry. The satellite to main-core peak separation is generally related to the amplitude of this monopolar transition.

The shake-up structures at 402.4 and 289.2 eV are respectively distant by 3.8 eV from the N 1s peak and 3.6 eV from the C 1s peak (related to carbons attached to nitrogens). The similarity of these separations suggests that the valence transition is located in the C=N bond region and occurs between two orbitals related to this bond, since the orbital whose density is localized near the atom where the initial hole is formed is most likely to be excited.[17] This hypothesis agrees with the strong C=N π-overlap population (Table I), and a valence transition starting from the $2b_{2g}$ π level seems most appropriate in the one-electron picture.

The satellites connected with the S 2p peaks have a smaller amplitude and are interpreted as transitions arising from the highest occupied molecular orbital (π $4b_{1u}$) located 1.4 eV below the Fermi level in the XPS spectrum. The absence of such a satellite near the N 1s peak is consistent with the low electron density between nitrogen and sulfur atoms as predicted by Mulliken analysis.

The existence of shake-up satellites associated with a C=N bond and their absence in the case of a N–S bond substantiates further the picture of high electron density in the C–N region and low electron density on the N–S bond.

(13) Riga, J.; Verbist, J. J.; Wudl, F.; Kruger, A. *J. Chem. Phys.* **1978**, *69*, 3221.

(14) Carlson, T. A. In "Photoelectron and Auger Spectroscopy"; Plenum Press, New York, 1975; p 241.

(15) Baker, A. D.; Brundle, C. R. In "Electron Spectroscopy"; Academic Press, New York, 1977; Vol. 1, 48.

(16) Martin, R. L.; Shirley, D. A. In "Electron Spectroscopy"; Academic Press, New York, 1977; Vol. 1, 86.

(17) Gelius, U.; Allan, C. J.; Allison, D. A.; Siegbahn, H.; Siegbahn, K. *Chem. Phys. Lett.* **1971**, *11*, 224.

Table IV. Core- and Valence-Peak Binding Energies of $(NSeN)_2$ (eV)

core peak	peak position	satellite position (intensity)
C 1s	284.4-285.5	
N 1s	398.2	399.4 (strong) 401.6 (low)
Se $3p_{3/2}$	162.7	
Se $3p_{1/2}$	168.4	

valence peak[a]	peak position	valence peak	peak position
A	1.4	E	10.9
B	3.6	F	15.0
C	6.2	G	17.4
D	8.9	H	22.5

[a] Peaks are labeled as in Figure 12.

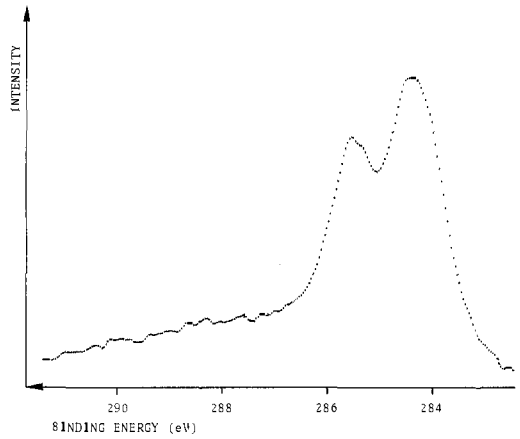

Figure 9. X-ray photoelectron spectrum of the C 1s level in $(NSeN)_2$.

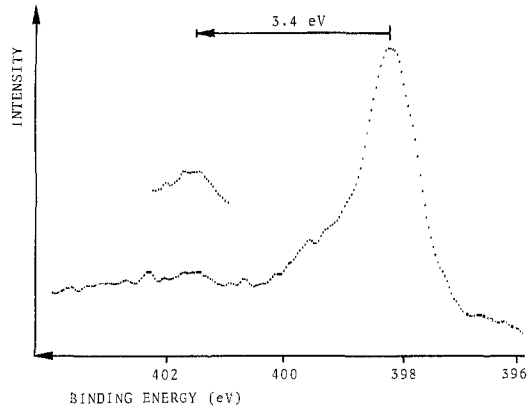

Figure 10. X-ray photoelectron spectrum of the N 1s level in $(NSeN)_2$.

B. $(NSeN)_2$. Core Levels. Their features are collected in Table IV. As in $(NSN)_2$, the C 1s peak is split into two components of 1.1-eV separation (Figure 9) reflecting the same pattern of charge distribution on the carbon atoms for both compounds. Replacement of sulfur by selenium does not drastically change the electron distribution of the naphthalene ring.

The N 1s peak (Figure 10) shifts toward lower binding energy, thus revealing an increase of electron density on the four nitrogens. Two satellites are observed; the most intense appears as a shoulder on the left-hand side of the main peak, the other being located at 401.6 eV.

The large Se $3p_{1/2}$ and Se $3p_{3/2}$ peak widths and the presence of intense Auger lines preclude any search and determination of satellites in this region (Figure 11). The binding energy by comparison with other seleno compounds[13] suggests partial positive charge on the selenium atoms.

Atomic charge distribution in $(NSN)_2$ and $(NSeN)_2$ have a similar picture.

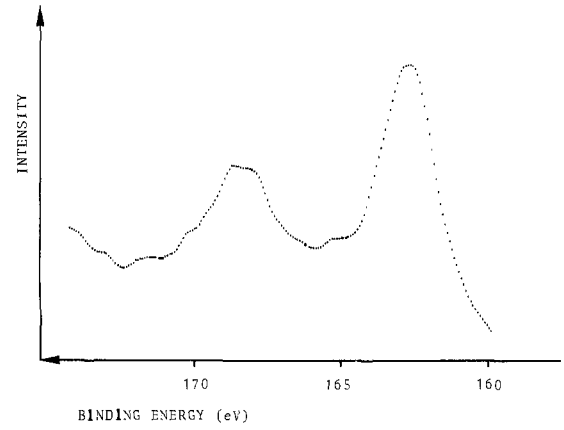

Figure 11. X-ray photoelectron spectrum of the Se 3p levels in $(NSeN)_2$.

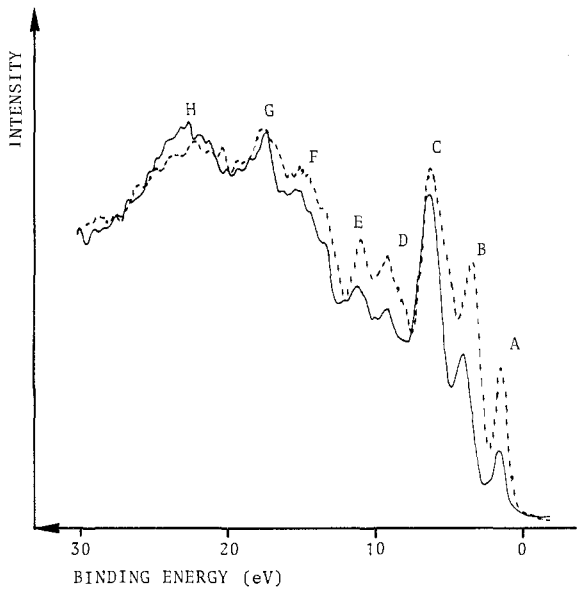

Figure 12. Comparison of the $(NSN)_2$ (—) and $(NSeN)_2$ (···) valence-band spectra.

Valence Levels. The valence levels of $(NSN)_2$ and $(NSeN)_2$ are compared in Figure 12, and their energy values are listed in Table IV.

Both the shapes of the two spectra and the observed binding energies are closely similar. While S 3s and Se 4s relative cross sections are nearly equal, those of S 3p and Se 4p[18] are quite distinct, and therefore intensity differences between $(NSN)_2$ and $(NSeN)_2$ are larger in the 0.0–12.0 eV region. In particular, the dominant chalcogen p character of the HOMO can be deduced from the large intensity of peak A.

Peak A has the same binding energy in $(NSeN)_2$ as in $(NSN)_2$, which rules out expectations of modifying properties depending on HOMO position by replacing S by Se.

Satellites. The presence of Se Auger peaks near 288 and 184 eV excludes the possibility of accurate observation of shake-up satellites in the C 1s and Se 3p regions. Only the N 1s satellite is visible at 401.6 eV, with a 3.4-eV separation from the main N 1s peak. As in $(NSN)_2$ we associate it with an electronic transition starting from the $2b_{2g}$ molecular orbital. We assume, by analogy with $(NSN)_2$, that a similar satellite connected with the C 1s line should exist but overlaps with the Se Auger line.

C. Shape of N 1s Core Peaks. In both compounds, the N 1s peak has a companion component distant by 1.0 eV on the high-energy side of the spectrum; its intensity is about one-third of the main peak. Several hypotheses can be considered for its origin: crystallographically different nitrogens, multiplet splitting, plasmons, sample degradation, shake-up satellite, etc.

(18) Scofield, J. H. *J. Electron Spectrosc. Relat. Phenom.* **1976**, *8*, 129.

According to their crystal structures,[3,19] both molecules have D_{2h} symmetry, implying four equivalent nitrogens. Intermolecular interactions alone cannot account for a chemical shift as large as 1.0 eV.

The multiplet splitting hypothesis requires the existence of a biradical that EPR measurements[2] do not support. Moreover the observed 1:3 ratio in the XPS N 1s line does not agree with the calculated 1:2 ratio in the case of a biradical.

Several works on $(SN)_x$ have reported plasmon excitations during photoemission.[20,21] Such collective oscillations need a conductive medium and may not be involved in the cases of $(NSN)_2$ and $(NSeN)_2$.

Sample degradation is unlikely. The chemical inertness of these compounds is well established.[2] Surface oxygen contamination remains negligible, and regular control of core-levels lines does not show any alteration under irradiation. Measurements performed under the same conditions at 4 months interval are perfectly reproducible.

The last possibility we have investigated was to attribute this component to a shake-up transition. In organic compounds, such as the lowest acenes, these transitions present a large amplitude (2-10 eV) and give rise to satellites of weak intensity, typically less than 10% of the main peak.[22] As the two highest occupied π levels ($4b_{1u}$ and $2b_{2g}$) have already been involved in the explanation of other shake-up features, this transition should start from the $6b_{1g}$ σ orbital having a strong nitrogen-lone-pair character. In a simplified picture, where molecular orbitals are assumed to relax similarly, there is a linear relation between satellite energies and excitation energies of valence electrons. In fact, this relation is not simple, and the orderings of valence excitations and their coresponding satellites can be very different.[23,24] Therefore, it is not unlikely that a satellite of low amplitude may originate in a transition starting from the deep $6b_{1g}$ orbital. However, a more detailed discussion on the nature, the amplitude, and the probability of this transition would need elaborate calculations beyond the scope of this paper.

Further work on compounds with similar NSN linkages is in progress to understand the N 1s peak shape.

Concluding Remarks

The parallel use of X-ray photoelectron spectroscopy and ab initio calculations, undertaken to characterize the electronic structure of $(NSN)_2$, has shown that (i) the nitrogen atoms are negatively charged while sulfurs and carbons linked to nitrogens are positive, (ii) compared to those of naphthalene, the highest occupied levels are strongly perturbed due to the adjunction of two NSN entities, and (iii) C=N has double-bond character, as shown from both shake-up satellites existence and Mulliken population analysis.

These results, in agreement with previous experimental results, suggest the quinonoid structure as the most accurate to describe the bonding in $(NSN)_2$ and $(NSeN)_2$. Sulfur 3d orbitals induce a partial back-donation of electrons from nitrogen to sulfur, thereby reducing the polarity of the NSN bond.

Substitution of sulfur by selenium does not bring any marked modification in the electronic structure, as is reflected by similar HOMO's in $(NSN)_2$ and $(NSeN)_2$.

Registry No. $(NSN)_2$, 65989-13-1; $(NSeN)_2$, 71248-50-5.

(19) Gieren, A.; Lamm, V.; Haddon, R. C.; Kaplan, M. L. *J. Am. Chem. Soc.* **1980**, *102*, 5070.
(20) Salaneck, W. R.; Lin, J. W.-P.; Epstein, A. J. *Phys. Rev. D* **1976**, *D13*, 5574.
(21) Brant, P.; Weber, D. C.; Ewing, C. T.; Carter, F. L.; Marshall, J. A. *Synth. Met.* **1979**, *1*, 161.
(22) Riga, J.; Pireaux, J. J.; Caudano, R.; Verbist, J. J. *Phys. Scr.* **1977**, *16*, 346.
(23) Cederbaum, L. S. *Mol. Phys.* **1974**, *28*, 479.
(24) Domcke, W.; Cederbaum, L. S.; von Niessen, W.; Kraemer, W. P. *Chem. Phys. Lett.* **1976**, *43*, 258.

Cadmium-113 NMR T_1 and Nuclear Overhauser Enhancement Measurements on Cadmium Cyclohexanediaminetetraacetate

Charles C. Bryden*[1] and Charles N. Reilley[†]

Contribution from the Kenan Laboratories of Chemistry, University of North Carolina, Chapel Hill, North Carolina 27514. *Received August 7, 1981*

Abstract: The ^{113}Cd NMR T_1 and nuclear Overhauser enhancement (NOE) have been measured for CdCyDTA in H_2O and D_2O solutions at 2.3 T. These measurements allowed the calculation of the dipole-dipole contribution to T_1, which was the same in both solutions. A selective NOE experiment was performed on the CdCyDTA solution in 100% H_2O, in which the water protons, the acetate methylene protons, and the methine protons were successively irradiated; only the irradiation of the CyDTA acetate methylene protons gave a detectable NOE. These results demonstrate that water does not penetrate the CdCyDTA inner coordination sphere and that the acetate methylene protons of CyDTA are the only protons which contribute to the dipolar portion of the ^{113}Cd T_1.

Recently considerable interest has been shown in obtaining information about metal-binding sites in zinc, calcium, and other metal-containing proteins via ^{113}Cd NMR of the Cd-substituted proteins.[2-5] As pointed out by Ellis et al.,[6] the study of simpler model systems by ^{113}Cd NMR is necessary in order to better interpret the results obtained on biological systems. The ^{113}Cd relaxation studies on the Cd aquo[7] and CdEDTA[6] complexes are important first steps toward the understanding of ^{113}Cd relaxation

[†] Deceased December 31, 1981.

(1) To whom correspondence should be addressed at Hercules, Inc., Research Center, Wilmington, DE 19899.
(2) Sudmeier, James L.; Bell, Stuart J. *J. Am. Chem. Soc.* **1977**, *99*, 4499-4500.
(3) Bailey, David B.; Ellis, Paul D.; Cardin, Alan D.; Behnke, W. David *J. Am. Chem. Soc.* **1978**, *100*, 5236-5237.

0002-7863/82/1504-2697$01.25/0